Beam Learning in MmWave/THz-band Drone Networks Under In-Flight Mobility Uncertainties

Sabarish Krishna Moorthy, *Student Member, IEEE* and Zhangyu Guan, *Senior Member, IEEE*

Abstract—This paper focuses on designing high-data-rate wireless communications for drone networks in the mmWave and terahertz (THz) frequency bands. MmWave/THz-band communications have been envisioned as key technologies to achieve ultra broadband wireless links through beamforming in 5G and beyond networks. However, a main challenge with these frequency bands is that the narrow-beam directional wireless links can be easily disconnected because of the beam misalignment in mobile environments. To address this challenge, in this paper we design a new beam control scheme called *LeBeam*, with the objective of maximizing the expected capacity of the mmWave/THz-band links by determining the optimal beamwidth dynamically under the mobility uncertainties of flying drones. In *LeBeam*, an Echo State Network (ESN) is adopted to capture the mobility uncertainties of the drones dynamically and predict the optimal beamwidth based on the first- and second-order moments of the drone mobility. The ESN has been trained based on real drone flight traces. To this end, we measure and analyze the mobility uncertainties of flying drones by carrying out a series of field experiments in different weather. It is found that flying drones experience micro-, small- and large-scale mobility uncertainties, and the resulting mobility behavior cannot be characterized with any existing statistical models. The performance of *LeBeam* is evaluated over UBSim, a newly developed trace-driven Universal Broadband Simulator for integrated aerial and ground wireless networking. Results indicate that the micro-scale mobility has only negligible effects on the link capacity (less than 1%), while the wireless links may experience significant capacity degradation (over 50% on average) in the presence of small- and large-scale mobility uncertainties.

Index Terms—Millimeter-wave and Terahertz Bands, Wireless Drone Networks, Beam control, Echo State Learning.

1 Introduction

This paper aims at designing broadband wireless drone networks in the millimeter-wave (mmWave) and Terahertz (THz) frequency bands. Mmwave/THz-band drone networks have been envisioned as a key technology to enable a wide set of new applications, including distributed beamforming with collaborative drones [2], distributed aerial edge computing [3], high-throughput and secure tactical wireless networking in contested environments [4], wireless backhauling for cellular networks with mobile hotspots [5]–[8], among others. However, radio in-air signal propagation in these frequency bands suffers from significantly high path loss ($0.3 - 1000$ dB/km) due to the absorption by water vapor and oxygen [9]. To overcome this problem[1], directional transmissions with narrow beams have been used to achieve extended communication distance [10]. The resulting mmWave/THz-band wireless links can be easily disconnected by the misalignment between the communicating nodes particularly in mobile environments.

To address this problem, beam search and alignment have attracted significant research attention in existing literature [11]–[15]. For example, BeamSpy [11] and Agile-Link [12] predict the best mmWave beam alignment without scanning the space thereby reducing the overhead and delay. In [13], Hashemi et. al design an optimal algorithm to reduce the overhead of beam alignment in mmWave systems. In [14], the authors propose to use the side information obtained from radar mounted on the static mmWave base station to adapt the beams of the vehicular communication system. Perfecto et al. [15] propose a framework to jointly consider the channel state information and queue state information to establish mmWave links. Please refer to [16], [17] and references therein for an excellent survey of the main results in this field.

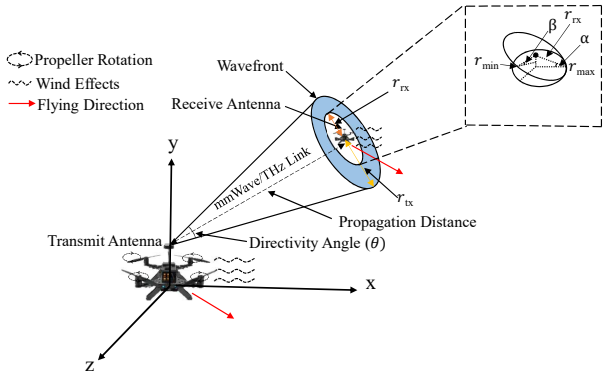

Fig. 1: Wireless communications between flying drones in the mmWave/THz bands with mobility uncertainties.

A preliminary shorter version of this paper appeared in the Proceedings of IEEE INFOCOM Workshop on Wireless Communications and Networking in Extreme Environments (WCNEE), Paris, France, April 2019 [1].
Sabarish Krishna Moorthy and Zhangyu Guan are with the Department of Electrical Engineering, University at Buffalo, The State University of New York, Buffalo, NY 14260. E-mail: {sk382, guan}@buffalo.edu.

1. It is worth mentioning that the distance problem with mmWave and THz-band communications can be partially addressed with UAVs, by dynamically deploying UAVs closer to each other or additional UAVs as relays. This is however out the scope of this paper.

The above discussed beam alignment schemes aim at identifying the transmit and receive beams that can result in the highest signal strength, without explicitly considering the challenges in wireless unmanned aerial vehicle (UAV) networks. The readers are referred to [18]–[22] and references therein for a survey of the potentials and challenges of wireless UAV networks. Differently, in this paper we aim at designing high-data-rate wireless drone networks in the mmWave/THz bands under in-flight mobility uncertainties. As illustrated in Fig. 1, in drone networks the drone may experience large-, small- and micro-scale mobility uncertainties, caused by the drone flight, wind effects, and engine operation and propeller rotation, respectively. On commercial 60 GHz mmWave routers, e.g., TP-Link Talon AD7200 [23], it may take tens of milliseconds to perform beam search. This is significantly slower than the micro-scale drone mobility and comparable with the small-scale mobility according to field measurements. Therefore, it is hard for the mmWave/THz links to recover from the beam misalignment through beam search.

The main contributions of the paper are as follows.

- We propose a new beam control scheme called *LeBeam*, with the objective of maximizing the mmWave/THz-band wireless links by dynamically determining the optimal beamwidth under multi-scale mobility uncertainties of the flying drones. In *LeBeam*, echo state network (ESN) learning is used to capture the dynamic mobility uncertainties of the flying drones and to determine dynamically the optimal beamwidth by jointly considering the communication distance and the first- and second-order statistical information of the drone mobility at network run time.
- A series of field experiments have been conducted to measure the mobility uncertainties of the flying drones in different weather conditions. Then, the ESN model is trained based on the drone mobility traces collected in the field experiments. The statistical behavior of the drone mobility has also been analyzed. It is found that no existing statistical models can be used to characterize the mobility uncertainties of the flying drones.
- The performance of *LeBeam* is evaluated through an extensive simulation campaign over UBSim, a newly developed trace-driven simulator for broadband aerial-ground networks. Results show that *LeBeam* can determine the optimal beamwidth with up to fair accuracy, and nearly optimal link capacity can be achieved under mobility uncertainties of the flying drones without requiring real-time beam alignment. All the data and code generated through the experiments have been released via GitHub [24].

The remainder of the paper is organized as follows. In Section 2 we discuss the related work. The system model is presented in Section 3. The design of *LeBeam* is presented in Section 4. We measure and analyze the mobility uncertainties of flying drones in Section 5. Finally, we discuss the simulation results in Section 6 and draw the main conclusions in Section 7.

2 Related Work

MmWave and THz-band has drawn significant research attention in existing literature [25]–[31] For example, in [25] Barati et al. reduce the latency and energy consumption required to establish mmWave link with fully digital front-end beamformers. In [26] the authors investigate the problem of concurrent transmission scheduling for THz wireless backhaul network. In [27], Saeed et al. study the feasibility of wireless communications over the THz-band at various atmospheric altitudes. In [28] Zhang et al. propose a novel framework to optimize the downlink communication of a mmWave Base Station with the help of reconfigurable intelligent reflector and distributional reinforcement learning. In [29], [30] Chaccour et al. investigate THz-band communications for Virtual Reality (VR) applications. For example, in [29] they propose a risk-based framework, which uses a recurrent neural network to optimize the rate and reliability of THz-band enabled cellular networks for VR applications. Barazideh et al. use in [31] reinforcement learning to detect and mitigate the intermittent interference for THz-enabled directional links.

There has also been significant research focusing on UAV aided mmWave/THz communications [32]–[37]. For example, the authors of [32] propose a tractable three-dimensional (3D) spatial model for evaluating the average downlink performance of UAV networks in the mmWave bands. Zhu et al. explore 3D beamforming in [33] for mmWave UAV communications with a phased uniform planar array. In [34], Gapeyenko et al. investigate the use of UAVs to mitigate the impact of blockage on the backhaul links. In [35], the authors evaluate the performance of UAV-assisted mmWave network in urban environments. In [36], Feng et al. propose a spectrum management architecture and evaluate its performance in UAV-assisted cellular networks. In [37] the authors address the challenge of establishing UAV-based mmWave links by deriving a tractable and closed-form statistical channel model for UAV communications, and show that the model can be used to find the optimal antenna directivity gain under different levels of UAV instability.

The beam misalignment problem has also been extensively studied in existing literature [38]–[44]. For example, in [38] Ke et al. propose a fast beam tracking scheme based on position prediction of multiple moving UAVs. In [39] the authors use fast beam tracking and self-healing mechanism to find alternate links as a possible solution to cope with the problem of beam misalignment in UAV network. In [40] Zhong et al. propose an improved beam tracking method to solve the problem of beam misalignment due to UAV movement. In [41], the authors study a mean field game approach

to address the challenge in establishing reliable and steady connections between flying UAVs, by adjusting the beam steering angle of the UAVs. In [42], the authors propose a fast beam tracking scheme to overcome the beam misalignment due to turning on and off the UAVs to enable energy efficient device-to-device communications. The problem of beam training and tracking for UAV mmWave communications was studied in [43] to achieve a trade-off between beam training quality and the training cost. In [44] Zhang et al. study codebook-based beam training for UAV mmWave communications.

Finally, Kovalchukov et al. [45] analyze the effects of directionality and random heights on UAV-based mmWave communications. In [46], Petrov et al. investigate the behavior of THz-band wireless links in the presence of small-scale mobility of the user. Please refer to [47]–[50] and references therein for an excellent survey of the main results in this field. None of these existing work has considered explicitly the multi-scale mobility uncertainties of the flying drones. Differently, the objective of our work is to achieve high-data-rate drone communications in the mmWave/THz bands under mobility uncertainties without relying on real-time beam alignment. We achieve this objective by making use of the statistical mobility information of UAV mobility uncertainties and use ESN based *LeBeam* to predict the optimal directivity angle which can be used to achieve high-data-rate communication.

3 System Model

Consider mmWave/THz-band wireless communications between two flying UAVs, Tx and Rx. An example of the target applications is backhaul communications in next-generation wireless networks with flying relays. The transmission time is divided into a set $\mathcal{T}$ of time slots. Define $\mathbf{cod}_{\rm tx}^t = (x_{\rm tx}^t,\ y_{\rm tx}^t,\ z_{\rm tx}^t)$ as the coordinate vector of UAV Tx in time slot $t \in \mathcal{T}$, with $x_{\rm tx}^t$, $y_{\rm tx}^t$ and $z_{\rm tx}^t$ being the x-, y- and z-axis components, respectively. Similarly, define $\mathbf{cod}_{\rm rx}^t = (x_{\rm rx}^t,\ y_{\rm rx}^t,\ z_{\rm rx}^t)$ as the coordinate vector of UAV Rx. Let η^t denote the SNR of the mmWave/THz-band link in time slot t, then the link capacity C^t can be written as

$$C^t = B\log_2(1+\eta^t), \tag{1}$$

where B is the bandwidth of the transmitted signal. To derive the mathematical expression of SNR η^t in (1), next we first describe the antenna and channel models.

Antenna Model. Since mmWave and THz bands undergo significant attenuation due to their small wavelength, it is undesirable to use omnidirectional antennas. Therefore, in this work we consider directional antennas to focus the signal energy into narrow beams and hence to extend the communication range. There are different models that can be used to characterize the behaviors of directional antennas, such as cone antenna model [51], which assumes perfect antenna radiation pattern with signal energy concentrated uniformly in the generated beam (i.e., no side lobes), and cone-plus-sphere antenna model [52], which considers side lobes as a sphere around the antenna. In this work, we consider as in [51] cone antenna model by assuming perfect antenna radiation pattern in favor of simpler modeling and analysis. It is worth pointing out that this work can also be extended to other more sophisticated directional antenna models such as cone-plus-sphere antenna model [52]. With cone antenna model, the transmit gain of the antenna can be defined as a function of the directivity angle, as the area of the wavefront of the transmit antenna increases with the directivity angle, which thereby reduces the transmit gain. Denote θ^t as the directivity angle[2] of the transmit antenna in time slot $t \in \mathcal{T}$, then the radius of the transmit wavefront, denoted as $r_{\rm tx}$, can be written as

$$r_{\rm tx} = \tan\left(\frac{\theta^t}{2}\right) d(\mathbf{cod}_{\rm rx}^t,\ \mathbf{cod}_{\rm tx}^t), \tag{2}$$

where $d(\mathbf{cod}_{\rm rx}^t, \mathbf{cod}_{\rm tx}^t)$ is the propagation distance defined as

$$d(\mathbf{cod}_{\rm rx}^t,\ \mathbf{cod}_{\rm tx}^t) = \sqrt{(x_{\rm rx}^t - x_{\rm tx}^t)^2 + (y_{\rm rx}^t - y_{\rm tx}^t)^2 + (z_{\rm rx}^t - z_{\rm tx}^t)^2}. \tag{3}$$

The area of the transmit wavefront, denoted as $A_{\rm tx}$, can then be given as

$$A_{\rm tx} = \pi r_{\rm tx}^2, \tag{4}$$

Without loss of generality, as illustrated in Fig. 1, consider drone Tx's location as the origin, i.e., $\mathbf{cod}_{\rm tx}^t = (0,\ 0,\ 0)$. Then the propagation distance $d(\mathbf{cod}_{\rm rx}^t,\ \mathbf{cod}_{\rm tx}^t)$ in (3) can be redefined as $d(\mathbf{cod}_{\rm rx}^t) \triangleq d(\mathbf{cod}_{\rm rx}^t,\ (0,\ 0,\ 0))$. The effective receive area of drone Rx's antenna depends on the time-varying relative locations as well as the rotation and inclination angles of the two drones.

Let α^t and β^t denote the relative roll and pitch angles of drone Rx's antenna with respect to y- and z-axis in time slot $t \in \mathcal{T}$, respectively. Then the receive area $A_{\rm rx}$ can be given as

$$A_{\rm rx} = \pi r_{\min} r_{\max} \tag{5}$$

where $r_{\min} = r_{\rm rx}\cos\beta^t$ and $r_{\max} = r_{\rm rx}\cos\alpha^t$ are the minor and major axes of the elliptical projection of receive antenna surface onto the y-z plane. Since in each time slot $t \in \mathcal{T}$ drone Rx's antenna may or may not overlap completely drone Tx's wavefront. Let $\mathcal{A}_{\rm tx}$ and $\mathcal{A}_{\rm rx}$ denote the set of points of the transmit and receive areas. Then the set of overlapping points can be defined as $\mathcal{A}_{\rm rx}^{\rm ovlp} \triangleq \mathcal{A}_{\rm tx} \cap \mathcal{A}_{\rm rx}$ with the corresponding overlapping area denoted as $A_{\rm rx}^{\rm ovlp}$.

Channel Model. In this work, we consider Line-of-Sight (LOS) communications between the UAVs. This is feasible because we consider that the UAVs are deployed at the same altitude, which is usually higher than that of the blockages (building, trees etc.) and hence the

2. In this paper, we use directivity angle and beamwidth interchangeably.

LOS link will dominate in the transmissions. In future work, this work can also be extended by considering other factors that affect the wireless channels, including different flight altitudes, Non-Line-of-Sight (NLOS) communications, blockage effects of the drone's body on the signal propagation, among others.

Let f denote the central frequency of the mmWave/THz-band wireless channel. For $f \in [f_0 - \frac{B}{2} \;\; f_0 + \frac{B}{2}]$, let $S_{\rm tx}(f)$ represent the single-sided power spectral density (p.s.d). Then the power of the transmitted signal at the receive antenna, denoted as $P_{\rm tx}$, can be given as

$$P_{\rm tx} = \lambda(\mathbf{cod}_{\rm rx}^t) \int_{f_0-\frac{B}{2}}^{f_0+\frac{B}{2}} S_{\rm tx}(f) df, \tag{6}$$

where $\lambda(\mathbf{cod}_{\rm rx}^t) = \frac{1}{A_{\rm tx}(\mathbf{cod}_{\rm rx}^t)}$ is the spreading attenuation coefficient with propagation distance $d(\mathbf{cod}_{\rm rx}^t)$, with $A_{\rm tx}(\mathbf{cod}_{\rm rx}^t) = A_{\rm tx}$ being the transmit wavefront area defined in (4).

The mmWave/THz-band frequency response of the wireless channel, denoted as $H(f, d(\mathbf{cod}_{\rm rx}^t))$ at frequency f and propagation distance $d(\mathbf{cod}_{\rm rx}^t)$, can be given as

$$H(f, d(\mathbf{cod}_{\rm rx}^t)) = \left| \frac{c}{4\pi d(\mathbf{cod}_{\rm rx}^t)} \int_{f_0-\frac{B}{2}}^{f_0+\frac{B}{2}} \frac{e^{-\frac{\mu(f) d(\mathbf{cod}_{\rm rx}^t)}{2}}}{f} df \right|^2, \tag{7}$$

where c is the speed of light and $\mu(f) \in \{\mu(f_{\rm mm}), \mu(f_{\rm tz})\}$ is the molecular absorption coefficient for mmWave/THz signal of frequency $f_{\rm mm}$ and $f_{\rm tz}$, respectively, with $\mu(f_{\rm mm}) < \mu(f_{\rm tz})$. In (7), $\mu(f)$ can be further defined as $e^{-K(f)d(\mathbf{cod}_{\rm rx}^t)}$ [51], where $K(f)$, representing the overall absorption coefficient, is a monotonically decreasing function of frequency f, and its values are available from the HITRAN database [53]. Then the received power at UAV Rx, denoted as $P_{\rm rx}$, can be expressed as [54]

$$P_{\rm rx} = A_{\rm rx}^{\rm ovlp} P_{\rm tx} H(f, d(\mathbf{cod}_{\rm rx}^t)) |H_{\rm rx}(f, d(\mathbf{cod}_{\rm rx}^t))|^2, \tag{8}$$

where $P_{\rm tx}$ and $H(f, d(\mathbf{cod}_{\rm rx}^t))$ are defined in (6) and (7), respectively; $H_{\rm rx}(f, d(\mathbf{cod}_{\rm rx}^t))$ denotes the frequency response of the receive antenna and is considered to be an ideal low-pass filter with bandwidth B.

Finally, the molecular absorption noise power at propagating distance $d(\mathbf{cod}_{\rm rx}^t)$, denoted as $N_{\rm rx}$, can be given as [55]

$$N_{\rm rx} = \int_{f_0-\frac{B}{2}}^{f_0+\frac{B}{2}} (S_{\rm back}(f) + S_{\rm self}) |H_{\rm rx}|^2 df, \tag{9}$$

where $S_{\rm back}(f)$ is the background atmospheric noise p.s.d, $S_{\rm self}$ is self-induced noise p.s.d, and $H_{\rm rx}$ is the receive antenna frequency response. Then, the SNR of the mmWave/THz link in time slot $t \in \mathcal{T}$, i.e., η^t in (1), can be given as

$$\eta^t = P_{\rm rx}/N_{\rm rx}, \tag{10}$$

with $P_{\rm rx}$ and $N_{\rm rx}$ defined in (8) and (9), respectively.

Problem Statement. Given central frequency f and bandwidth B of the mmWave/THz-band wireless channel, the location trajectory of the drones $\{(\mathbf{cod}_{\rm tx}^t, \mathbf{cod}_{\rm rx}^t)\}$ as well as the trajectory of the relative angle of the drone antennas $\{(\alpha^t, \beta^t)\}$, the beam control problem can be formalized as in (11).

$$\begin{aligned} Given: &\quad f, B, \{(\mathbf{cod}_{\rm tx}^t, \mathbf{cod}_{\rm rx}^t)\}, \{(\alpha^t, \beta^t)\}, \; t \in \mathcal{T} \\ Find: &\quad \{\theta^t\}, \; t \in \mathcal{T} \\ Maximize: &\quad \tfrac{1}{|\mathcal{T}|} \sum_{t \in \mathcal{T}} C^t(\theta^t) \\ Subject\ to: &\quad \theta^{\min} \le \theta^t \le \theta^{\max} \end{aligned} \tag{11}$$

where $|\cdot|$ represents the cardinality of a set, $C^t(\theta^t)$ is the link capacity defined through (1) to (10), and $\theta^{\min}$ and $\theta^{\max}$ denote the minimum and maximum directivity angle values, respectively.

The objective of network control problem (11) is to determine the beamwidth (i.e., directivity angle θ in Fig. 1) of the transmit drone beam that can maximize the average capacity of the mmWave/THz link in (11). As discussed above, the directivity angle is one of the key factors that affect the link capacity. On one hand, larger angle results in larger transmit wavefront area $A_{\rm tx}$ and hence lower power density $S_{\rm tx}(f)$ in (6) and lower received SNR η^t in (10). On the other hand, smaller angle leads to smaller effective receiving area $A_{\rm rx}^{\rm ovlp}$ and hence will cause more frequent misalignment between the transmit and receive antennas. In the case of misalignment, beam recovery schemes can be adopted to restore the links, e.g., on demand alignment and periodic alignment [56], fast alignment [12] and unimodal beam alignment [13]. Let $t_{\rm bal}$ denote the time taken for the beam recovery procedure, which we refer to as beam alignment latency in the rest of the paper.

4 Stochastic Beam Control

The main challenges in solving problem (11) are i) the location and angle of the drones are time-varying random variables and hence the optimal beamwidth cannot be determined in advance; ii) it is impractical to adapt the beamwidth θ^t based on instantaneous location and relative angle information of the drones, which may cause significant communication overhead. As of today, the effects of the mobility uncertainties of flying drones on mmWave/THz-band wireless communications is still unexplored. To address these challenges, in this section we propose a learning-based stochastic beam control scheme called *LeBeam*, which determines the optimal beamwidth through echo state learning based on the statistical drone mobility information.

Overall Architecture. In this work, we design LeBeam based on Echo State Network (ESN) learning.ESN is a type of reservoir computing, which has emerged recently as an alternative to the traditional gradient descent methods for training recurrent neural networks (RNN) [57]. In ESN, only the output weight matrix needs to be trained, while the weight matrices for the input and the

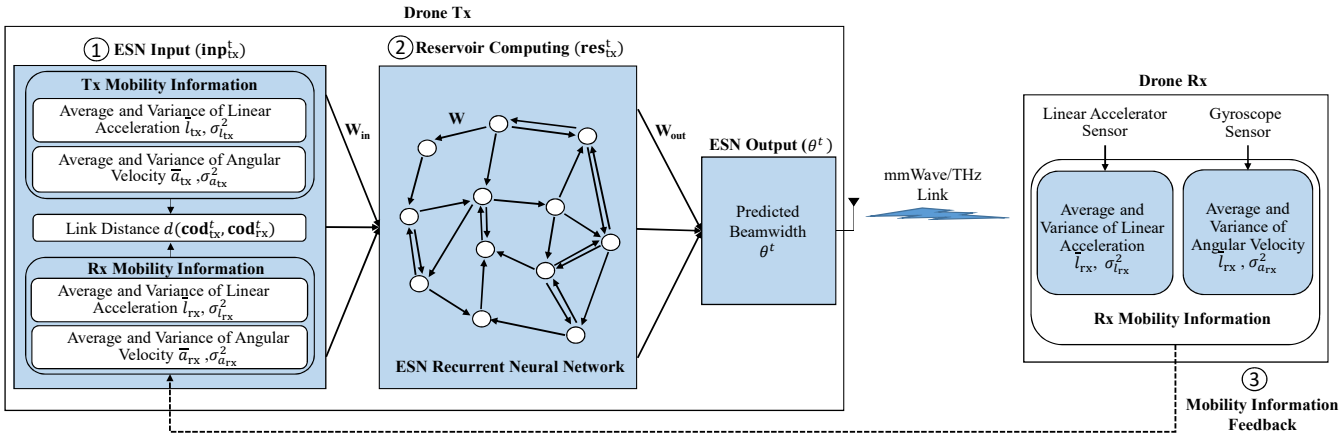

Fig. 2: LeBeam: Learning-based Stochastic Beam Control.

hidden layers can be generated randomly without any specific training. In this work, we consider as in [58]–[63] ESN because it is computationally inexpensive and has been shown to be a highly practical approach to RNN training, and hence are more suitable for wireless network control with network devices of limited computing capabilities (which are drones in our case).

The diagram of *LeBeam* is illustrated in Fig. 2. Drone Tx first constructs *ESN Input* in Step ①, which consists of the mobility information of the communicating drones. *ESN Input* is then fed to the ESN recurrent neural network for *Reservoir Computing* (Step ②). The *ESN Output* of the reservoir computing is the predicted optimal beamwidth θ^t in time slot t. In Step ①, Drone Rx's mobility information is collected through *Mobility Information Feedback* (Step ③). Next we describe the three steps sequentially.

ESN Input. LeBeam determines dynamically the optimal beamwidth based on statistical mobility information of the communicating drones. As illustrated in Step ① in Fig. 2, The *ESN Input* consists of the link distance between Drones Tx and Rx, the average and variance of the location displacement of Drones Tx and Rx, and the average and variance of the roll, pitch and yaw angles of the drones. In this work, we consider the average and variance of the linear and angular displacement values as input of the ESN, because we are interested in designing light-weight beam control schemes that require as few signaling exchanges as possible between the transmit and receive drones. This is motivated by the observation that, in the presence of micro- and small-scale mobility uncertainties, the drone's instantaneous location and orientation may change very fast, e.g., 200 times per second according to our measurements; as a result, feeding back instantaneous displacement values may cause significant communication overhead. Here, the link distance can be calculated based on the average linear acceleration information received by Drone Tx from Drone Rx.

The location displacement of drones Tx and Rx at time slot $t+1$ with respect to time slot t can be expressed respectively as

$$l^{t+1}_{\rm tx}=\sqrt{(x^{t+1}_{\rm tx}-x^t_{\rm tx})^2+(y^{t+1}_{\rm tx}-y^t_{\rm tx})^2+(z^{t+1}_{\rm tx}-z^t_{\rm tx})^2}, \quad (12)$$

$$l^{t+1}_{\rm rx}=\sqrt{(x^{t+1}_{\rm rx}-x^t_{\rm rx})^2+(y^{t+1}_{\rm rx}-y^t_{\rm rx})^2+(z^{t+1}_{\rm rx}-z^t_{\rm rx})^2}. \quad (13)$$

Then, the average location displacement, denoted respectively as $\bar{l}_{\rm tx}$ and $\bar{l}_{\rm rx}$ for Drones Tx and Rx, can be given as

$$\bar{l}_{\rm tx}=\frac{1}{\mathcal{T}}\sum_{t\in\mathcal{T}} l^{t+1}_{\rm tx}, \quad (14)$$

$$\bar{l}_{\rm rx}=\frac{1}{\mathcal{T}}\sum_{t\in\mathcal{T}} l^{t+1}_{\rm rx}. \quad (15)$$

The corresponding variance of the location displacement, denoted as $\sigma^2_{l_{\rm tx}}$ and $\sigma^2_{l_{\rm rx}}$, can be written as

$$\sigma^2_{l_{\rm tx}}=\frac{1}{\mathcal{T}}\sum_{t\in\mathcal{T}}(l^{t+1}_{\rm tx}-\bar{l}_{\rm tx})^2, \quad (16)$$

$$\sigma^2_{l_{\rm rx}}=\frac{1}{\mathcal{T}}\sum_{t\in\mathcal{T}}(l^{t+1}_{\rm rx}-\bar{l}_{\rm rx})^2. \quad (17)$$

Similarly, let $(\alpha^t_{\rm tx}, \beta^t_{\rm tx}, \gamma^t_{\rm tx})$ and $(\alpha^t_{\rm rx}, \beta^t_{\rm rx}, \gamma^t_{\rm rx})$ denote the roll, pitch and yaw angles of Drone Rx at time slot t, and $(\alpha^{t+1}_{\rm tx}, \beta^{t+1}_{\rm tx}, \gamma^{t+1}_{\rm tx})$ and $(\alpha^{t+1}_{\rm rx}, \beta^{t+1}_{\rm rx}, \gamma^{t+1}_{\rm rx})$ denote the angles at time slot $t+1$. Then the average (denoted respectively as $\bar{a}_{\rm tx}$ and $\bar{a}_{\rm rx}$ for Drones Tx and Rx) and variance (denoted as $\sigma^2_{a_{\rm tx}}$ and $\sigma^2_{a_{\rm rx}}$) of the angles can be calculated similarly as in (14)-(17).

Finally, the input to the ESN at time t, represented as $\mathbf{inp}^t_{\rm tx}$, can be defined as

$$\mathbf{inp}^t_{\rm tx}=(d(\mathbf{cod}^t_{\rm tx},\mathbf{cod}^t_{\rm rx}),\bar{l}_{\rm tx},\bar{l}_{\rm rx},\sigma^2_{l_{\rm tx}},\sigma^2_{l_{\rm rx}},\bar{a}_{\rm tx},\bar{a}_{\rm rx},\sigma^2_{a_{\rm tx}},\sigma^2_{a_{\rm rx}},\theta^t_{\rm tgt}), \quad (18)$$

where $\theta^t_{\rm tgt}$ is the target directivity angle in time slot t and is needed only for training the ESN. In this work, $\theta^t_{\rm tgt}$ is obtained based on grid search in the training phase (which will be further discussed in Section 5).

Reservoir Computing. In echo state learning a reservoir acts as a nonlinear high-dimensional expansion and a memory of input $\mathbf{inp}_{\text{tx}}^t$ [57]. We design *LeBeam* based on reservoir computing because it can provide a rich and relevant enough signal space $\mathbf{res}_{\text{tx}}^t \in \mathbb{R}^{N_{\text{res}}}$ with N_{res} being the dimension of the reservoir units, in which the desired output θ_{tgt}^t can be represented by linear combination of $\mathbf{inp}_{\text{tx}}^t$ and $\mathbf{res}_{\text{tx}}^t$. Let N_{inp} and N_{out} denote the dimension of the input and output units, respectively. Given the training input signal $\mathbf{inp}^t \in \mathbb{R}^{N_{\text{inp}}}$ and the target output signal $\theta_{\text{tgt}}^t \in \mathbb{R}^{N_{\text{out}}}$, the objective of learning scheme in the training phase is to learn a model with output θ^t that minimizes the root-mean-square error (RMSE) between θ^t and θ_{tgt}^t, defined as

$$E(\theta^t, \theta_{\text{tgt}}^t) = \frac{1}{N_{\text{out}}} \sum_{i=1}^{N_{\text{out}}} \sqrt{\frac{1}{|\mathcal{T}|} \sum_{t=1}^{|\mathcal{T}|} (\boldsymbol{\theta}^t - \theta_{\text{tgt}}^t)^2}, \tag{19}$$

where $|\cdot|$ represents the cardinality of a set.

For the signal space $\mathbf{res}_{\text{tx}}^t$, our learning scheme uses a Recurrent Neural Network (RNN) with leaky-integrated discrete-time continuous-value units. Let $\mathbf{W_{in}} \in \mathbb{R}^{N_{\text{res}} \times (1+N_{\text{inp}})}$ and $\mathbf{W} \in \mathbb{R}^{N_{\text{res}} \times N_{\text{res}}}$ denote the input and reservoir weight matrices, respectively. Further let $\delta \in (0, 1]$ denote the leaking rate. Then, the signal space $\mathbf{res}_{\text{tx}}^t$ can be updated as

$$\widetilde{\mathbf{res}}_{\text{tx}}^t = \tanh(\mathbf{W_{in}}[1; \mathbf{inp}_{\text{tx}}^t] + \mathbf{W}\mathbf{res}_{\text{tx}}^{t-1}), \tag{20}$$

$$\mathbf{res}_{\text{tx}}^t = (1-\delta)\, \mathbf{res}_{\text{tx}}^{t-1} + \delta\, \widetilde{\mathbf{res}}_{\text{tx}}^t \tag{21}$$

where $\tanh(\cdot)$ is the transfer function, and $[\cdot;\cdot]$ stands for matrix concatenation operation. Then the output θ^t can be given as

$$\theta^t = \mathbf{W_{out}}[1; \mathbf{inp}_{\text{tx}}^t; \mathbf{res}_{\text{tx}}^t], \tag{22}$$

where $\mathbf{W_{out}} \in \mathbb{R}^{N_{out} \times (1+N_{\text{inp}}+N_{\text{res}})}$ is the output weight matrix of the ESN.

Mobility Information Feedback. As illustrated in Step ③ in Fig. 2, Drone Rx feeds back its mobility information to Drone Tx. This includes the average and variance of acceleration information measured by the linear accelerator sensor and the angular information of the receive antenna measured by the gyroscope sensor. It is worth pointing out that, the feedback can be accomplished via either in-band or out-band channels and we assume that the feedback is error free, e.g., by using strong channel coding protection or retransmissions. This assumption is reasonable because, as mentioned earlier in this section, in this work we are interested in designing light-weight beam control schemes since the statistical information of the drones' mobility changes slowly with time and no frequent feedback is needed. The experiment setup for drone mobility measurements and the ESN training will be further discussed in Section 5.

5 Field Measurement and ESN Training

Recall that θ_{tgt}^t in (18) and (19) represents the target beamwidth, which is needed during the training phase of *LeBeam*. In *LeBeam*, θ_{tgt}^t is obtained based on grid search with mobility traces of flying drones collected through a series of field experiments.

Mobility Measurement. The experimental setup is shown in Fig. 3. In the experiments, an Intel Aero Ready-to-Fly (RtF) drone [64] is used to carry an Android smartphone with inbuilt linear acceleration and gyroscope sensors[3]. Sensor Kinetics Pro App is used to

3. In this work we consider Intel Aero RtF drones each of weight 865 g without batteries to measure the in-flight mobility uncertainties. In future work, we will consider other commercial drones to capture the impact of the drone's weight on the in-flight mobility uncertainties and hence the quality of the wireless links in the mmWave and THz bands, e.g., DJI Mavic Air 2 [65] and DJI Matrix Pro [66] with weight of 570 g and 5930 g (without batteries), respectively.

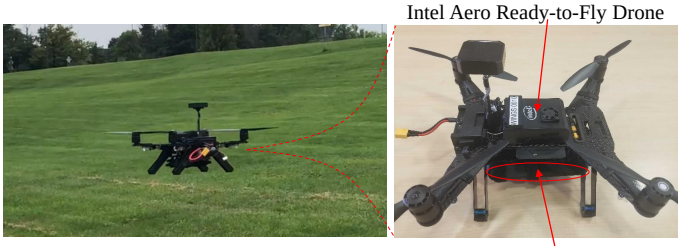

Fig. 3: Field measurement of drone flight uncertainties.

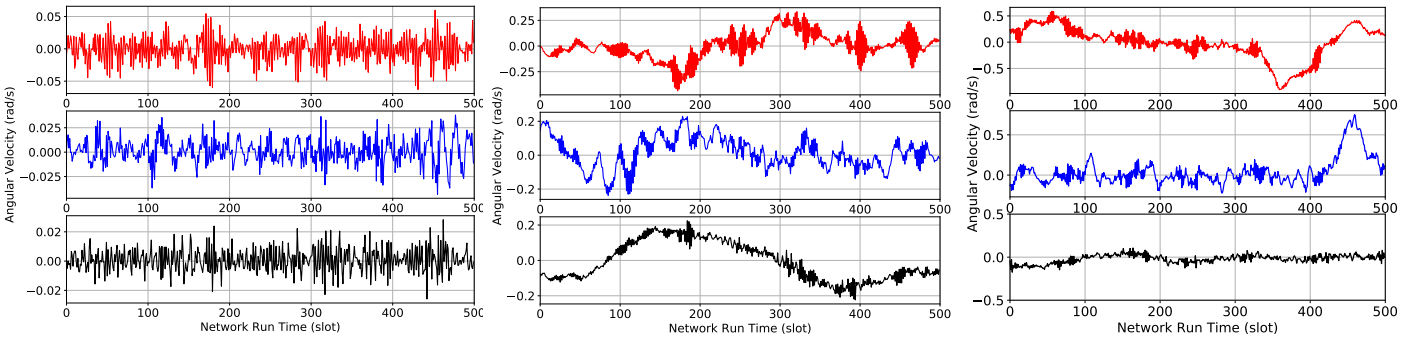

(a) (b) (c)

Fig. 4: Examples of drone mobility traces with (a) micro-, (b) small- and (c) large-scale uncertainties in windy weather. The top, middle and bottom subfigures correspond to the roll, pitch and yaw dimensions of the trace, respectively.

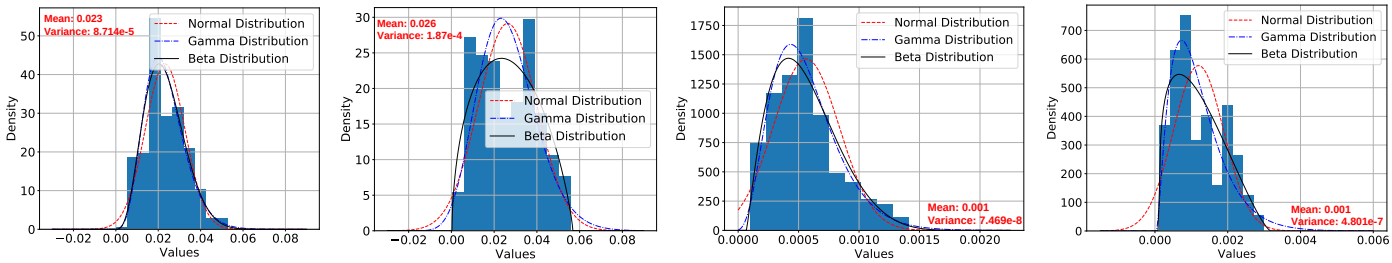

(a) (b) (c) (d)

Fig. 5: Statistical behavior of the measured drone mobility. (a): Linear displacement, small-scale, windy; (b) Linear displacement, large-scale, windy; (c) angular displacement, small-scale, windy; and (d) angular displacement, large-scale, windy.

Weather Condition	Mobility Pattern	Linear Acceleration	Angular Velocity
Windy	Micro-scale	Traces 1 - 20	Traces 121 - 140
	Small-scale	Traces 21 - 40	Traces 141 - 160
	Large-scale	Traces 41 - 60	Traces 161 - 180
Non-Windy	Micro-scale	Traces 61 - 80	Traces 181 - 200
	Small-scale	Traces 81 - 100	Traces 201 - 220
	Large-scale	Traces 101 - 120	Traces 221 - 240

TABLE 1: Data set of drone mobility traces collected during the field measurements for linear acceleration and angular velocity in different weather conditions.

Mobility Uncertainty	KS Test			
	Linear Displacement		Angular Displacement	
	Statistic	p-value	Statistic	p-value
Small-scale Non-Windy	0.50001	0.00777	0.50009	0.00776
Large-scale Non-Windy	0.50012	0.00776	0.50083	0.00763
Small-scale Windy	0.50011	0.00776	0.50011	0.00776
Large-scale Windy	0.50014	0.00775	0.50036	0.00771

TABLE 2: Kolmogorov-Smirnov statistical hypothesis testing

record the measured mobility data, including the angular velocity of the orientation and rotation of drone, and the acceleration of the drone movement excluding the effect of gravity of Earth.

The experiments are conducted in outdoor environments with different weather conditions: *non-windy day* and *windy day*. In each weather condition, we measure the micro-, small- and large-scale mobility uncertainties of the drone, caused by the engine operation and propeller rotation, the disturbance when hovering, and the in-flight instability, respectively. A set of 240 drone mobility traces have been collected, with 120 traces for each weather condition. Each trace lasts 5 seconds, with the sampling rate configured to 200 Hz for the gyroscope and linear acceleration sensors. Figures 4(a)-(c) give the examples of the angular velocity traces of the drone in windy weather condition with micro-, small- and large-scale mobility uncertainties, respectively. In each figure, the top, middle and bottom subfigures plot the roll, pitch and yaw angular velocity (in rad/s) of the drone, respectively, with each time slot corresponding to a sampling period (5 ms). From Fig. 4(a) it can be seen that, as expected, in the presence of only micro-scale mobility the drone experiences very frequent fluctuations but in a very small range (up to 0.05 rad/s). Differently, the fluctuations resulting from small- and large-scale mobility are in obviously larger ranges as shown in Figs. 4(b) and (c). The resulting data set is summarized in Table 1 and has been made available via GitHub [24].

We further calculate the linear displacement and angular displacement in different time slots and fit their distributions with existing statistical models, including normal, gamma and beta distributions. Examples of the fitting results are reported in Figs. 5(a) and (b) for linear displacement with small- and large-scale mobility uncertainties in windy environments and Figs. 5(c) and (d) for the angular displacement. It can be found that it is hard to use these statistical models to characterize the multi-scale mobility uncertainties of flying drones in different scenarios. For example, the beta distribution fits best the small-scale linear displacement with small-scale mobility in Fig. 5(a) but not in Fig. 5(b) with large-scale mobility. Similarly, the gamma distribution fits the angular displacement in Fig. 5(c) but not for Fig. 5(d). We further test the accuracy of the fitting by conducting statistical hypothesis testing for linear displacement and angular displacement. We consider Kolmogorov-Smirnov Test [67] as an example, while other approaches can also be adopted such as Chi-square Test [68]. The results are reported in Table 2 for normal distribution based fitting, while the results are similar for the other distributions. It can be seen that the p-value in all the tested cases is less than 0.05, a threshold below which it means that the data does not fit well normal distribution. As a result, the optimal expected link capacity in (11) cannot be derived in closed-form in the presence of drone mobility with unknown and time-varying distributions. This motivated us to capture the statistical behavior of the drone mobility through ESN learning in the design of *LeBeam*. Next we describe how to train the ESN based on the collected drone mobility traces.

LeBeam Training. Recall in (18) that in the training phase of *LeBeam*, in addition to the statistical drone mobility information we also need to feed the target beamwidth θ^t_{tgt} to the ESN reservoir computing. In *LeBeam* this is accomplished by grid searching the op-

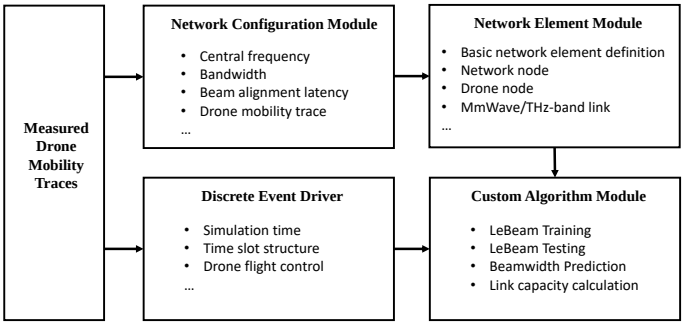

Fig. 6: UBSim Diagram.

timal beamwidth for a subset of the collected drone mobility traces, while the rest of the traces are used for testing. Specifically, given a training mobility trace, we first perform grid search for each time slot t with directivity angles θ varying from 1 degree to 75 degrees with step of 1 degree. For each angle, we calculate the transmit wavefront and receiving areas given by (4) and (5), respectively. We then obtain the overlapping area which will be used to obtain the transmit power given by (6) and ultimately obtain the SNR given by (10), based on which we can further calculate the capacity given by (1). This process is repeated for all the time slots. Then, we determine the directivity angle that achieves the maximum capacity and use it as the target directivity angle θ^t_{tgt}. The input and output weights of *LeBeam* is updated such that the RMSE in (19) is minimized. In Section 6, we will test the performance of the trained ESN model by considering the rest of the collected drone mobility traces.

6 Performance Evaluation

We evaluate the performance of *LeBeam* proposed in Section 4 in terms of beamwidth prediction accuracy and the achievable link capacity. In the experiments the center frequency and bandwidth for the mmWave band is set to 30 GHz and 1 GHz, respectively. For the THz band, the center frequency is set to 300 GHz and the bandwidth is set to 10 GHz. The transmit power for mmWave and THz bands are set to 500 mW and 20 mW, respectively. It is worth pointing out that we consider both mmWave and THz bands because, on one hand, we want to show that

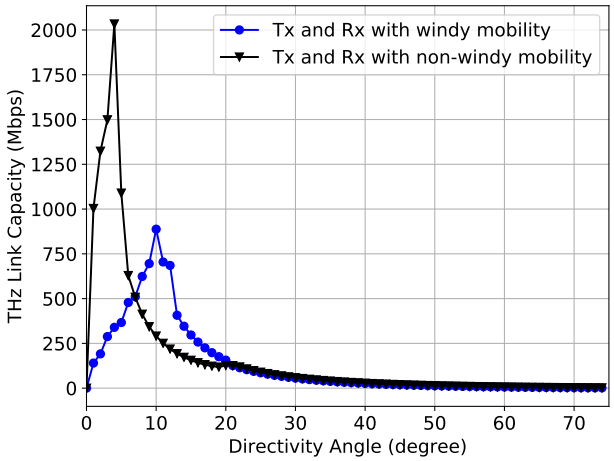

Fig. 7: Link capacity with different beam directivity angles.

our beam control algorithm proposed in Sections 4 and 5 is not limited to any specific frequency band, and on the other hand, we expect to understand how differently the two spectrum bands perform in the presence of in-flight mobility uncertainties. Moreover, it is also important for many emerging applications to operate on both mmWave and THz frequency bands [50], [69]–[71]. For example, in next-generation (i.e., 5G and Beyond) wireless networks with drone base stations, while mmWave communications can be used for fronthaul links, the backhaul links can operate on both mmWave and THz bands. The experiments are conducted over UBSim, a newly developed discrete network simulator driven by flight traces for broadband aerial-ground wireless networking. Next, we first briefly introduce the design of UBSim, and then present the simulation results including the effects of mobility uncertainties on link capacity, prediction accuracy of *LeBeam*, as well as the effects of directivity angles and beam alignment latency (BAL).

UBSim Development. UBSim is a Python-based trace-driven simulator for broadband integrated aerial-ground wireless networks. As shown in Fig. 6, UBSim comprises of four modules: *Network Configuration Module (NCM)*, *Network Element Module (NEM)*, *Discrete Event Driver (DED)*, and *Custom Algorithm Module (CAM)*. Through the NCM module, one can configure various network parameters, including the bandwidth of each spectrum

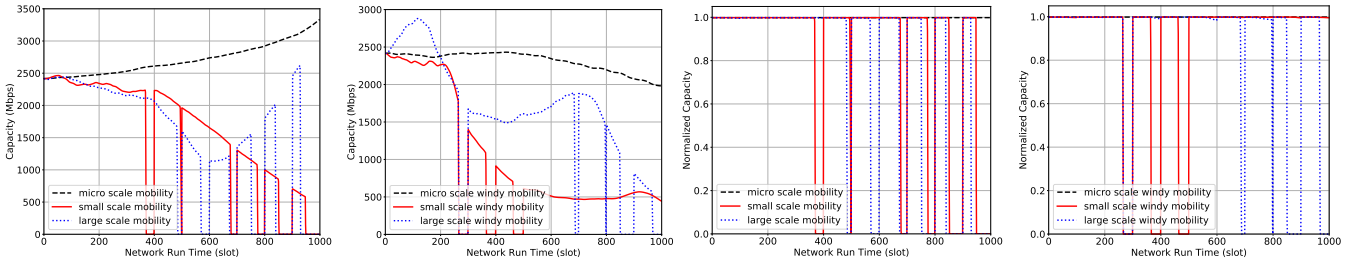

Fig. 8: Effects of different mobility uncertainties on link capacity in non-windy and windy weather. (a) and (b): Actual Capacity; (c) and (d): Normalized Capacity.

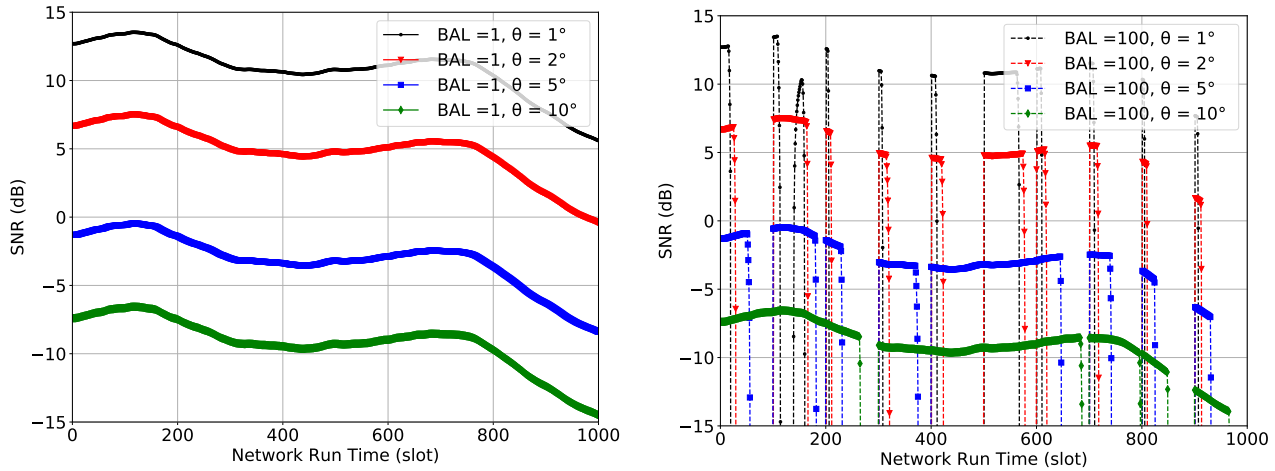

(a) (b)

Fig. 9: Link SNR with different beam alignment latency (BAL) (a) BAL = 1, (b) BAL = 100.

band, the transmission power of the nodes, and the drone mobility traces to use, among others. The NEM module defines the classes for all the network elements, including Network, Flying Drone Hotspots, Links among others. These classes have been designed in a hierarchical manner. At the highest level is a general network element class net_elmt, which defines the basic network element attributes and operations such as registering an element in the network, specifying the parent and children elements of an element. The DED module provides the discrete network simulation environment based on the open-source library SimPy [72]. Finally, the CAM module hosts the custom-designed network control algorithms (*LeBeam* in this work).

Link Capacity With Mobility Uncertainties. We first study the effects of directivity angle on the wireless link capacity taking the THz band as an example, We consider one mobility traces for windy and non-windy weather, respectively. The directivity angle is varied from 1 to 75 degrees with step of 1 degree. For each angle, the link capacity is averaged over all the time slots for each mobility trace. The results are reported in Fig. 7. It can be seen that when drones are flying in non-windy environments, the maximum THz link capacity (around 2 Gbps) is achieved with directivity angle of 4°. Differently, when they are flying in windy weather the maximum capacity (around 1 Gbps) is achieved with directivity angle of 10°. This is because in windy environments the drones experience more frequent small-scale fluctuations, and larger directivity angles can lead to lower link outage probability. This verifies the importance of dynamically adapting the directivity angle to the drone's mobility uncertainties.

Figure 8 shows the effects of different mobility uncertainties on the link capacity. We consider a total simulation time of 1000 slots, with each time slot of 5ms. The beamwidth is set to 10° and the beam alignment latency is set to 100 slots, i.e., 0.5s. We consider THz-frequency band, and plot the actual link capacity in Figs. 8(a) and 8(b) and the normalized capacity in Figs. 8(c) and 8(d). The normalized capacity is obtained by dividing the actual link capacity by the capacity achieved with perfect antenna alignment (or no misalignment). It can be seen that the wireless link can maintain an average capacity of 2711 Mbps in the presence of only micro-scale mobility caused by the vibration of the engine operation and propeller rotation. This corresponds to normalized capacity of 1, as shown in Figs. 8(c) and 8(d). Differently, in the case of small- and large-scale mobility, the wireless link experiences an outage soon after the experiment starts. For example, in Figs. 8(a) and (c) we can see that the link capacity as well as the normalized link capacity undergoes frequent fluctuations due to beam misalignment. *This implies that the negative effects of micro-scale mobility uncertainties on the link capacity can be safely ignored*. For example, no adaptive beamforming scheme will be needed when the drones are just landed while their engines are still operating, because they experience only micro-scale mobility in that case. This also implies that in the case of general mobility it is sufficient to perform beamforming adaptations at the time scale of small-scale rather than micro-scale mobility.

Figure 9 reports the effects of directivity angles on the wireless link quality in terms of SNR with different beam alignment latency (BAL), taking the THz band and mobility uncertainty in windy weather as an example, while similar results can be obtained for mmWave band. We consider BAL of 1 and 100 time slots (corresponding to 5 ms and 500 ms, respectively) and calculate the SNR of the THz link with directivity angles of 1, 2, 5 and 10 degrees. With BAL of 1 time slot, the average SNR (around 10.85 dB) is achieved with directivity angle of 1°. This is because the THz link can recover from the misalignment almost in real time, and hence higher SNR can be achieved by transmitting with smaller directivity angle to concentrate better the signal energy. However, with BAL of 100 time slots (i.e., 500 ms), we can see that the THz-band link is disconnected frequently (with prob-

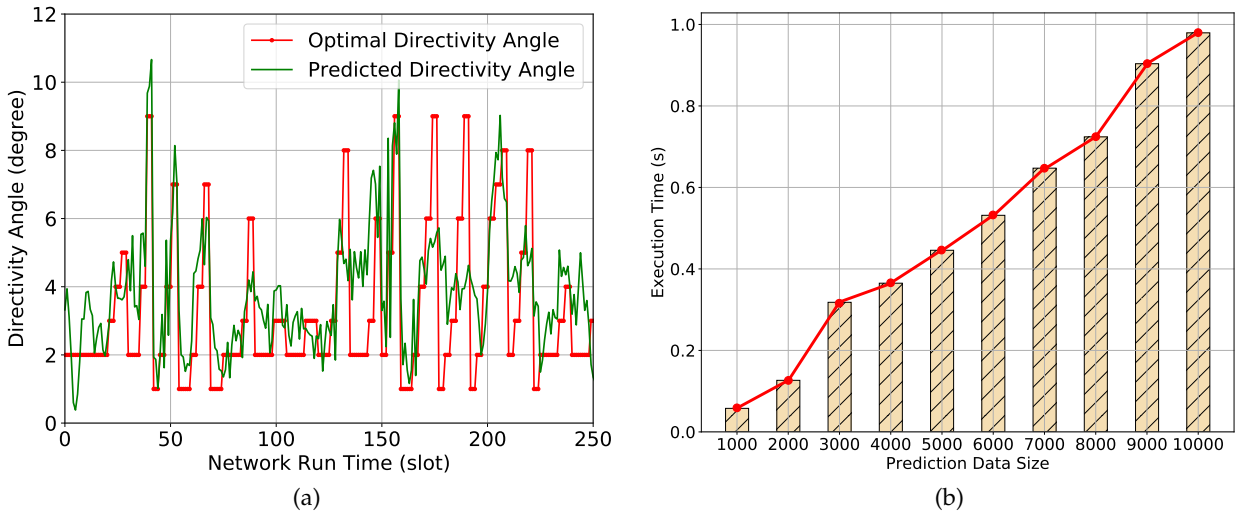

(a) (b)

Fig. 10: Effectiveness of *LeBeam*. (a) large scale, windy.; (b) Complexity Analysis of *LeBeam* for large scale, windy.

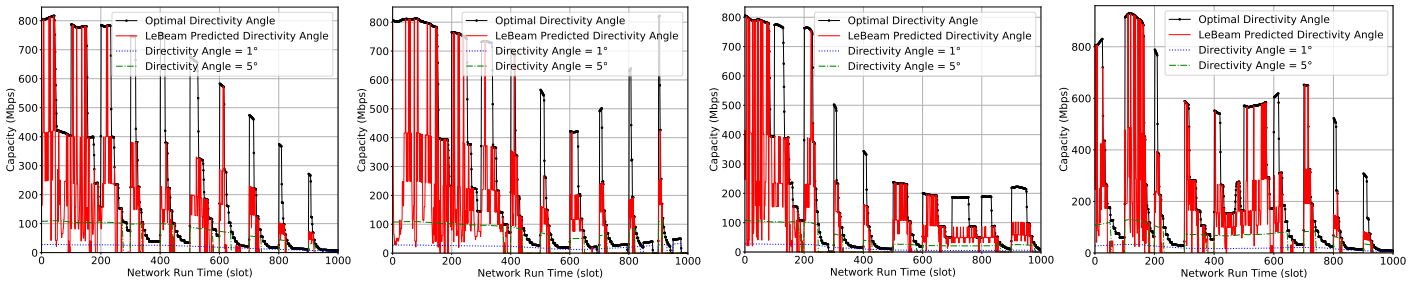

(a) (b) (c) (d)

Fig. 11: MmWave-band link capacity with different directivity angles. (a) Small scale, non-windy; (b) large scale, non-windy; (c) small scale, windy; and (d) large scale, windy.

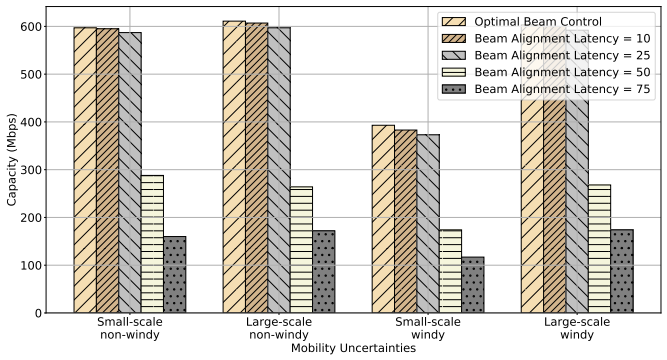

Fig. 12: mmWave band Link capacity with different beam alignment latency.

ability of 13%-82%), because of the misalignment caused by the large- and small-scale mobility of the UAVs in windy weather. Recall that in the above experiments no adaptive beamwidth control (i.e., *LeBeam*) has been adopted. In the following experiments we will test the effectiveness of the proposed *LeBeam* scheme.

Effectiveness and Complexity of LeBeam. In this experiment we verify the effectiveness of the proposed *LeBeam* scheme in terms of prediction accuracy. To this end, the ESN model in LeBeam is trained as described in Section 4 using the drone mobility traces collected in Section 5, and validated based on k-fold cross validation [73]. A total of 60 traces for each weather condition was obtained with 20 traces for each mobility pattern. In the training and validation phases, we select a random trace from the mobility trace dataset (Table 1) for each mobility pattern and weather condition, while the remainder of the dataset is used for testing. The selected trace contains 1000 drone trajectory samples, i.e., 1000 samples with sampling rate of 200 Hz. The measurement for the two weather conditions were conducted on different days using the same drone and android smart phone to account for any calibration errors. Figure 10(a) shows an example of the LeBeam validation results, where it can be seen that *LeBeam* can predict effectively the optimal directivity angle.

We further study the complexity of *LeBeam* algorithm. The experiments are conducted on a workstation with Intel(R) Core(TM) $i7-10510U$ CPU @ 1.80 GHz 2.30 GHz, memory of 16.0 GB, and 64-bit Windows Operating System. The results are reported in Fig. 10(b) where we plot the execution time of *LeBeam* as a function of data sample size. It can be seen that the complexity of *LeBeam* in terms of execution time increases linearly with the data size.

MmWave Link Capacity with LeBeam. In the following set of experiments, we will evaluate the effectiveness of LeBeam in the presence of BAL. To this end, we compare *LeBeam* with benchmark directivity angles of 1°

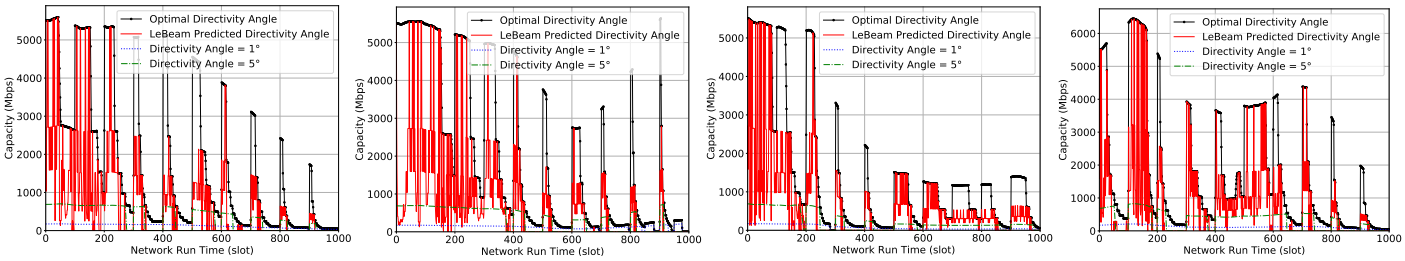

Fig. 13: THz-band link capacity with different directivity angles. (a) Small scale, non-windy; (b) large scale, non-windy; (c) small scale, windy; and (d) large scale, windy.

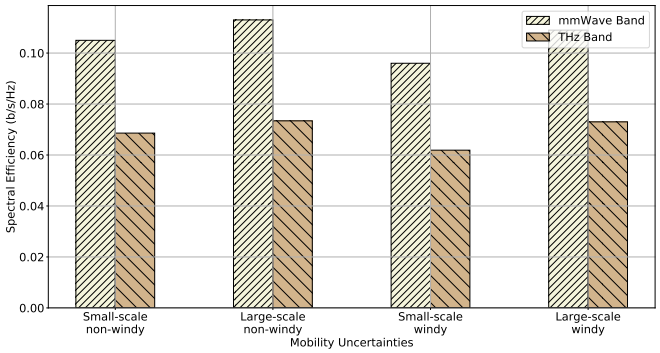

Fig. 14: Comparison of spectral efficiencies for mmWave and THz bands.

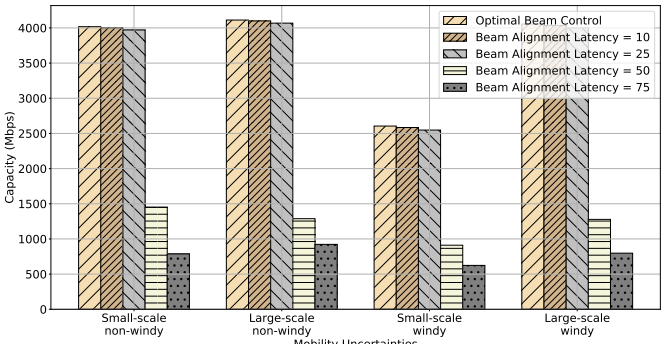

Fig. 15: THz band Link capacity with different beam alignment latency.

and 5°. Additionally, to show the optimality of LeBeam we perform grid search to determine the optimal angle at each time slot and obtain the corresponding capacity. This capacity is used as the upper bound for performance analysis. The beam alignment latency is set to 100 time slots (i.e., 500 ms). The results are reported in Fig. 11 for the mmWave band. It can be seen that significant capacity gain can always be achieved by LeBeam. For example, in Fig. 11 LeBeam can achieve capacities of 105 Mbps, 113 Mbps, 96 Mbps and 109 Mbps for the mmWave band with small-scale non-windy, large-scale non-windy, small-scale windy and large-scale windy uncertainties, respectively. With fixed directivity angle, e.g., 5°, the corresponding capacities are only 50 Mbps, 51 Mbps, 36 Mbps and 49 Mbps, respectively which on average is 2.3 times less compared to LeBeam.

We further verify the robustness of *LeBeam* in the presence of different beam alignment latency. We plot the capacity achieved by *LeBeam* with beam alignment latency of 1, 10, 25, 50 and 75 time slots. The case with latency of 1 time slot (5 ms) is considered as the optimal beam control scheme. The results for mmWave band are reported in Fig. 12 by averaging over the entire testing duration of 1000 time slots. We can see that nearly optimal capacity can be achieved with beam alignment latency of up to 25 time slots (i.e., 125 ms) in non-windy as well as windy environments. However, when the beam alignment latency increases to 50 time slots, the capacity decreases by 54% on average (51%, 56%, 53% and 55% for the four uncertainty cases, respectively). Similarly, the average decrease in capacity is 70% with beam alignment latency of 75 time slots.

THz Link Capacity with LeBeam. Similar results can be obtained for the THz band as reported in Figs. 13 and 15. Comparing Fig. 13 with Fig. 11, it can be found that with 10 times larger bandwidth than the mmWave band, the THz-band link can achieve on average 6.5 times higher capacity than the mmWave band, which is $6.53, 6.49, 6.45, 6.46$ times in Figs. 13(a), (b), (c), (d), respectively. The resulting overall spectral efficiency are plotted in Fig. 14. In Fig. 15, we further plot the link capacity of the THz link with different beam alignment latency. Similar to Fig. 12, nearly optimal capacity can also be achieved by *LeBeam* on the THz band with BAL of up to 25 time slots. However, with BAL of 50 and 75 time slots the decrease in capacity is 66% and 80%, respectively. This means that, as expected, the THz band is affected more in the presence of higher BAL compared to mmWave band.

7 Conclusions

In this paper we have studied the effects of mobility uncertainties on mmWave/THz-band communications between flying drones. The mobility uncertainties of the flying drones were characterized based on a series of field measurements. The link capacity of the mmWave/Thz links has been analyzed in the presence of micro-, small- and large-scale mobility uncertainties. It is found that, without adaptive beamwidth control, the micro-scale mobility has only negligible effects on

the link capacity (less than 1%), while the wireless links experience significant capacity degradation (over 50% on average) in the presence of small- and large-scale mobility uncertainties. To address this problem, we have proposed a stochastic beam control scheme *LeBeam*, which can predict the optimal beamwidth based on the first- and second-order moments of the drone mobility. Through an extensive simulation campaign, we showed that *LeBeam* can effectively predict the optimal directivity angle. Moreover, it is shown that good performance can be achieved by *LeBeam* in the presence of low- and moderate-level beam alignment latency, e.g., nearly optimal link capacity can be achieved by *LeBeam* if the latency is less than 125 ms. The dataset of the drone flight traces and source code generated through the experiments have been released to the community via GitHub [24].

REFERENCES

[1] Z. Guan and T. Kulkarni, "On the Effects of Mobility Uncertainties on Wireless Communications Between Flying Drones in the mmWave/THz Bands," in *Proc. of IEEE INFOCOM Workshop on Wireless Commun. and Networking in Extreme Environments (WCNEE)*, Paris, France, April 2019.

[2] Z. Guan, N. Cen, T. Melodia, and S. Pudlewski, "Self-Organizing Flying Drones with Massive MIMO Networking," in *Proc. of Mediterranean Ad Hoc Networking Workshop (Med-Hoc-Net)*, Capri, Italy, June 2018.

[3] N. Cheng et al., "Air-Ground Integrated Mobile Edge Networks: Architecture, Challenges and Opportunities," *IEEE Commun. Magazine*, vol. 56, no. 8, pp. 26–32, August 2018.

[4] L. Zhang, Z. Guan, and T. Melodia, "United Against the Enemy: Anti-Jamming Based on Cross-Layer Cooperation in Wireless Networks," *IEEE Transactions on Wireless Commun.*, vol. 15, no. 8, pp. 5733–5747, Aug 2016.

[5] I. Bor-Yaliniz and H. Yanikomeroglu, "The New Frontier in RAN Heterogeneity: Multi-Tier Drone-Cells," *IEEE Communications Magazine*, vol. 54, no. 11, pp. 48–55, Nov. 2016.

[6] H. Wang et al., "Power Control in UAV-Supported Ultra Dense Networks: Communications, Caching, and Energy Transfer," *IEEE Commun. Magazine*, vol. 56, no. 6, pp. 28–34, June 2018.

[7] Y. Zeng et al., "Wireless Communications with Unmanned Aerial Vehicles: Opportunities and Challenges," *IEEE Commun. Magazine*, vol. 54, no. 5, pp. 36–42, May 2016.

[8] Z. Guan, N. Cen, T. Melodia, and S. Pudlewski, "Joint Power, Association and Flight Control for Massive-MIMO Self-Organizing Flying Drones," *IEEE/ACM Transactions on Networking*, accepted for publication.

[9] G. A. Siles, J. M. Riera, and P. G. del Pino, "Atmospheric Attenuation in Wireless Communication Systems at Millimeter and THz Frequencies [Wireless Corner]," *IEEE Antennas and Propagation Magazine*, vol. 57, no. 1, pp. 48–61, Feb 2015.

[10] K. Heimann et al., "On the Potential of 5G mmWave Pencil Beam Antennas for UAV Communications: An Experimental Evaluation," in *Proc. of 22nd International ITG Workshop on Smart Antennas (WSA)*, Bochum, Germany,, March 2018.

[11] S. Sur et al., "BeamSpy: Enabling Robust 60 GHz Links Under Blockage," in *Proc. of Symposium on Networked Systems Design and Implementation (NSDI 16)*, Santa Clara, CA, March 2016.

[12] H. Hassanieh et al., "Fast Millimeter Wave Beam Alignment," in *Proc. of Conference of the ACM Special Interest Group on Data Commun.*, Budapest, Hungary, August 2018.

[13] M. Hashemi et al., "Efficient Beam Alignment in Millimeter Wave Systems Using Contextual Bandits," in *Proc. of IEEE Conference on Computer Commun. (ICC)*, Honolulu, HI, April 2018.

[14] N. González-Prelcic, R. Méndez-Rial, and R. W. Heath, "Radar aided beam alignment in mmWave V2I communications supporting antenna diversity," in *Proc. of Information Theory and Applications Workshop (ITA)*, La Jolla, CA, USA, Jan. 2016.

[15] C. Perfecto, J. D. Ser, and M. Bennis, "Millimeter-Wave V2V Communications: Distributed Association and Beam Alignment," *IEEE Journal on Selected Areas in Commun.*, vol. 35, no. 9, pp. 2148–2162, Sep. 2017.

[16] S. Kutty and D. Sen, "Beamforming for Millimeter Wave Communications: An Inclusive Survey," *IEEE Commun. Surveys Tutorials*, vol. 18, no. 2, pp. 949–973, December 2016.

[17] M. Xiao, S. Mumtaz, Y. Huang, L. Dai, Y. Li, M. Matthaiou, G. K. Karagiannidis, E. Björnson, K. Yang, C. I, and A. Ghosh, "Millimeter Wave Communications for Future Mobile Networks," *IEEE Journal on Selected Areas in Commun.*, vol. 35, no. 9, pp. 1909 – 1911, Sept. 2017.

[18] M. Chen, U. Challita, W. Saad, C. Yin, and M. Debbah, "Artificial Neural Networks-Based Machine Learning for Wireless Networks: A Tutorial," *arXiv:1710.02913*, 2017. [Online]. Available: https://arxiv.org/abs/1710.02913

[19] M. Mozaffari, A. T. Z. Kasgari, W. Saad, M. Bennis, and M. Debbah, "Beyond 5G With UAVs: Foundations of a 3D Wireless Cellular Network," *IEEE Transactions on Wireless Commun.*, vol. 18, no. 1, pp. 357–372, Jan. 2019.

[20] B. Li, Z. Fei, and Y. Zhang, "UAV Communications for 5G and Beyond: Recent Advances and Future Trends," *IEEE Internet of Things Journal*, vol. 6, no. 2, pp. 2241–2263, April 2019.

[21] Y. Zeng, Q. Wu, and R. Zhang, "Accessing From the Sky: A Tutorial on UAV Communications for 5G and Beyond," *Proceedings of the IEEE*, vol. 107, no. 12, pp. 2327–2375, Dec. 2019.

[22] M. Mozaffari, W. Saad, M. Bennis, Y. Nam, and M. Debbah, "A Tutorial on UAVs for Wireless Networks: Applications, Challenges, and Open Problems," *IEEE Commun. Surveys Tutorials*, vol. 21, no. 3, pp. 2334–2360, Mar. 2019.

[23] "TP-Link. 2018. talon ad7200 multi-band router." [Online]. Available: . http://www.tp-link.com/en/products/details/AD7200.html. (2018)

[24] https://github.com/ubwingslab/new-spectrum-technology.

[25] C. N. Barati, S. Dutta, S. Rangan, and A. Sabharwal, "Energy and Latency of Beamforming Architectures for Initial Access in mmWave Wireless Networks," *arXiv:2001.02034*, 2020. [Online]. Available: https://arxiv.org/abs/2001.02034

[26] H. Jiang, Y. Niu, B. Ai, Z. Zhong, and S. Mao, "QoS-Aware Bandwidth Allocation and Concurrent Scheduling for Terahertz Wireless Backhaul Networks," *IEEE Access*, vol. 8, pp. 125 814–125 825, 2020.

[27] A. Saeed, O. Gurbuz, and M. A. Akkas, "Terahertz Communications at Various Atmospheric Altitudes," *Physical Communication (Elsevier)*, vol. 41, 2020.

[28] Q. Zhang, W. Saad, and M. Bennis, "Millimeter Wave Communications with an Intelligent Reflector: Performance Optimization and Distributional Reinforcement Learning," *arXiv:2002.10572*, 2020. [Online]. Available: https://arxiv.org/abs/2002.10572

[29] C. Chaccour, M. N. Soorki, W. Saad, M. Bennis, and P. Popovski, "Risk-Based Optimization of Virtual Reality over Terahertz Reconfigurable Intelligent Surfaces," *arXiv:2002.09052*, 2020. [Online]. Available: https://arxiv.org/abs/2002.09052

[30] ——, "Can Terahertz Provide High-Rate Reliable Low Latency Communications for Wireless VR?" *arXiv:2005.00536*, 2020. [Online]. Available: https://arxiv.org/abs/2005.00536

[31] R. Barazideh, O. Semiari, S. Niknam, and B. Natarajan, "Reinforcement Learning for Mitigating Intermittent Interference in Terahertz Communication Networks," *arXiv:2003.04832*, 2020. [Online]. Available: https://arxiv.org/abs/2003.04832

[32] W. Yi, Y. Liu, M. Elkashlan, and A. Nallanathan, "Modeling and Coverage Analysis of Downlink UAV Networks with mmWave Communications," in *Proc. of IEEE International Conference on Commun. Workshops (ICC Workshops)*, Shanghai, China, May 2019.

[33] L. Zhu, J. Zhang, Z. Xiao, X. Cao, D. O. Wu, and X. Xia, "3-D Beamforming for Flexible Coverage in Millimeter-Wave UAV Communications," *IEEE Wireless Commun. Letters*, vol. 8, no. 3, pp. 837–840, June 2019.

[34] M. Gapeyenko, V. Petrov, D. Moltchanov, S. Andreev, N. Himayat, and Y. Koucheryavy, "Flexible and Reliable UAV-Assisted Backhaul Operation in 5G mmWave Cellular Networks," *IEEE Journal on Selected Areas in Commun.*, vol. 36, no. 11, pp. 2486–2496, Nov 2018.

[35] Z. Khosravi, M. Gerasimenko, S. Andreev, and Y. Koucheryavy, "Performance Evaluation of UAV-Assisted mmWave Operation in Mobility-Enabled Urban Deployments," in *Proc. of International Conference on Telecommunications and Signal Processing (TSP)*, Athens, Greece, July 2018.

[36] Z. Feng, L. Ji, Q. Zhang, and W. Li, "Spectrum Management for mmWave Enabled UAV Swarm Networks: Challenges and Opportunities," *IEEE Commun. Magazine*, vol. 57, no. 1, pp. 146–153, Jan 2019.
[37] M. T. Dabiri, H. Safi, S. Parsaeefard, and W. Saad, "Analytical Channel Models for Millimeter Wave UAV Networks under Hovering Fluctuations," *IEEE Transactions on Wireless Commun.*, vol. 19, no. 4, pp. 2868–2883, April 2020.
[38] Y. Ke et al., "Position Prediction Based Fast Beam Tracking Scheme for Multi-User UAV-mmWave Communications," in *Proc. of IEEE International Conference on Commun. (ICC)*, Shanghai, China, May 2019.
[39] P. Zhou, X. Fang, Y. Fang, R. He, Y. Long, and G. Huang, "Beam Management and Self-Healing for mmWave UAV Mesh Networks," *IEEE Transactions on Vehicular Technology*, vol. 68, no. 2, pp. 1718–1732, Feb. 2019.
[40] W. Zhong, L. Xu, Q. Zhu, X. Chen, and J. Zhou, "MmWave beamforming for UAV Communications with Unstable Beam Pointing," *China Commun.*, vol. 16, no. 1, pp. 37–46, Jan. 2019.
[41] Q. Cheng et al., "Beam-Steering Optimization in Multi-UAVs mmWave Networks: A Mean Field Game Approach," in *Proc. of International Conference on Wireless Commun. and Signal Processing (WCSP)*, Xi'an, China, Oct. 2019.
[42] Z. Zhang, Q. Zhu, and P. Zhang, "Fast Beam Tracking Discontinuous Reception for D2D-Based UAV mmWave Communication," *IEEE Access*, vol. 7, pp. 110 487–110 498, Aug. 2019.
[43] W. Zhang and W. Zhang, "Beam Training and Tracking Efficiency Analysis for UAV mmWave Communication," in *Proc. of IEEE International Conference on Communication Systems (ICCS)*, Chengdu, China, Dec. 2018.
[44] W. Zhang, W. Zhang, and S. Zhang, "Location Information Based Beam Training for UAV mmWave System," in *Proc. of IEEE/CIC International Conference on Commun. in China (ICCC)*, Changchun, China, Aug. 2019.
[45] R. Kovalchukov et al., "Analyzing Effects of Directionality and Random Heights in Drone-based mmWave Communication," *IEEE Transactions on Vehicular Technology*, vol. 67, no. 10, pp. 10 064–10 069, Oct. 2018.
[46] V. Petrov, D. Moltchanov, Y. Koucheryavy, and J. M. Jornet, "The Effect of Small-Scale Mobility on Terahertz Band Communications," in *Proc. ACM/IEEE International Conference on Nanoscale Computing and Commun. (NanoCom)*, Reykjavik, Iceland, Sept. 2018.
[47] Z. Xiao, P. Xia, and X. G. Xia, "Enabling UAV Cellular with Millimeter-Wave Communication: Potentials and Approaches," *IEEE Commun. Magazine*, vol. 54, no. 5, pp. 66–73, May 2016.
[48] Mumtaz, Shahid et al., "Terahertz Communication for Vehicular Networks," *IEEE Trans. on Vehicular Technology*, vol. 66, no. 7, pp. 5617–5624, July 2017.
[49] X. Wang et al., "Millimeter Wave Communication: A Comprehensive Survey," *IEEE Commun. Surveys Tutorials*, vol. 20, no. 3, pp. 1616–1653, thirdquarter 2018.
[50] K. M. S. Huq, S. A. Busari, J. Rodriguez, V. Frascolla, W. Bazzi, and D. C. Sicker, "Terahertz-Enabled Wireless System for Beyond-5G Ultra-Fast Networks: A Brief Survey," *IEEE Network*, vol. 33, no. 4, pp. 89–95, July 2019.
[51] V. Petrov et al., "Interference Analysis of EHF/THF Communications Systems with Blocking and Directional Antennas," in *Proc. of IEEE GLOBECOM*, Singapore, Dec. 2016.
[52] H. Chu and P. Xu, "Mutual Interference-based Relay Selection and Transmission Scheme for mmWave Wireless Networks," in *Proc. of International Conference on Wireless Commun. and Signal Processing*, Hangzhou, China, Oct. 2013.
[53] L. S. Rothman et al., "HITRAN: High-Resolution Transmission Molecular Absorption Database Harvard-Smithson Center for Astrophysics," 2014. [Online]. Available: https://www.cfa.harvard.edu/hitran/
[54] J. M. Jornet and I. F. Akyildiz, "Channel Modeling and Capacity Analysis of Electromagnetic Wireless Nanonetworks in The Terahertz Band," *IEEE Transactions on Wireless Commun.*, vol. 10, no. 10, pp. 3211–3221, Oct. 2011.
[55] ——, "Femtosecond-long Pulse-based Modulation for Terahertz Band Communication in Nanonetworks," *IEEE Trans. on Commun.*, vol. 62, no. 5, pp. 1742–1754, May 2014.
[56] V. Petrov, D. Moltchanov, Y. Koucheryavy, and J. M. Jornet, "Capacity and Outage of Terahertz Communications with User Micro-mobility and Beam Misalignment," *IEEE Transactions on Vehicular Technology*, vol. 69, no. 6, June 2020.
[57] M. Lukoševičius, "A Practical Guide to Applying Echo State Networks," *Lecture Notes*, Jan. 2012.
[58] H. Peng, C. Chen, C.-C. Lai, L.-C. Wang, and Z. Han, "A Predictive On-Demand Placement of UAV Base Stations Using Echo State Network," *arXiv:1909.11598*, 2019. [Online]. Available: https://arxiv.org/abs/1909.11598
[59] O. A. Adeleke, "Echo-State Networks for Network Traffic Prediction," in *Proc. of IEEE Information Technology, Electronics and Mobile Communication Conference (IEMCON)*, Vancouver, BC, Canada, Oct. 2019.
[60] X. Yang and F. Zhao, "Echo State Network and Echo State Gaussian Process for Non-Line-of-Sight Target Tracking," *IEEE Systems Journal*, pp. 1–8, April 2020.
[61] M. Chen, O. Semiari, W. Saad, X. Liu, and C. Yin, "Federated Echo State Learning for Minimizing Breaks in Presence in Wireless Virtual Reality Networks," *IEEE Transactions on Wireless Commun.*, vol. 19, no. 1, pp. 177–191, Jan. 2020.
[62] M. Chen, W. Saad, C. Yin, and M. Debbah, "Echo State Networks for Proactive Caching in Cloud-Based Radio Access Networks With Mobile Users," *IEEE Transactions on Wireless Commun.*, vol. 16, no. 6, pp. 3520–3535, June. 2017.
[63] M. Chen, W. Saad, and C. Yin, "Echo State Networks for Self-Organizing Resource Allocation in LTE-U With Uplink–Downlink Decoupling," *IEEE Transactions on Wireless Commun.*, vol. 16, no. 1, pp. 3–16, Jan. 2017.
[64] "Intel Ready to Fly Drone." [Online]. Available: https://www.intel.com/content/www/us/en/support/articles/000023272/drones/development-drones.html
[65] "Mavic Air 2 Drone." [Online]. Available: https://www.dji.com/mavic-air-2/specs
[66] "Matrice 600 Pro Drone." [Online]. Available: https://www.dji.com/matrice600-pro/info
[67] "Kolmogorov-Smirnov Test." [Online]. Available: https://docs.scipy.org/doc/scipy/reference/generated/scipy.stats.kstest.html
[68] "Chi-square Test." [Online]. Available: https://docs.scipy.org/doc/scipy/reference/generated/scipy.stats.chisquare.html
[69] R. Singh and D. Sicker, "Reliable THz Communications for Outdoor based Applications- Use Cases and Methods," in *Proc. of IEEE Consumer Commun. Networking Conference (CCNC)*, Las Vegas, NV, Jan. 2020.
[70] H. Elayan, O. Amin, R. M. Shubair, and M. Alouini, "Terahertz Communication: The Opportunities of Wireless Technology Beyond 5G," in *Proc. of International Conference on Advanced Communication Technologies and Networking (CommNet)*, Marrakech, Morocco, April 2018.
[71] H. Sarieddeen, N. Saeed, T. Y. Al-Naffouri, and M. Alouini, "Next Generation Terahertz Communications: A Rendezvous of Sensing, Imaging, and Localization," *IEEE Commun. Magazine*, vol. 58, no. 5, pp. 69–75, 2020.
[72] "Simpy." [Online]. Available: https://pypi.org/project/simpy/
[73] M. Lukoševičius and A. Uselis, "Efficient Cross-Validation of Echo State Networks," in *Proc. of Artificial Neural Networks and Machine Learning – ICANN 2019: Workshop and Special Sessions*. Cham: Springer International Publishing, 2019, pp. 121–133.

Sabarish Krishna Moorthy is a Ph.D. student in the Department of Electrical Engineering at State University of New York at Buffalo, NY, USA. He is currently working in the UB Wireless Intelligent Networking and Security Lab under the supervision of Professor Zhangyu Guan. He received his B.E. degree in Electronics and Communication Engineering from Velammal Engineering College, Chennai, India in 2016, and M.S. degree in Electrical Engineering from SUNY Buffalo in 2018. His research interests are in network design automation and new spectrum technologies.

Zhangyu Guan (SM'20) received the Ph.D. degree in Communication and Information Systems from Shandong University in China in 2010. He is currently an Assistant Professor with the Department of Electrical Engineering at the State University of New York at Buffalo, where he directs the Wireless Intelligent Networking and Security (WINGS) Lab, with research interests in network design automation, new spectrum technologies, and wireless network security. He has served as an Area Editor for Elsevier Journal of Computer Networks since July 2019. He has served as TPC chair for IEEE INFOCOM Workshop on Wireless Communications and Networking in Extreme Environments (WCNEE) 2020, Student Travel Grants Chair for IEEE Sensor, Mesh and Ad Hoc Communications and Networks (SECON) 2019-2020, Information System (EDAS) Chair for IEEE Consumer Communications Networking Conference (CCNC) 2021. He has also served as TPC member for IEEE INFOCOM 2016-2020, IEEE GLOBECOM 2015-2020, IEEE MASS 2017-2019, IEEE IPCCC 2015-2019, among others.